JOURNAL OF MATERIALS SCIENCE **40** (2005) 5801–5811

Investigation on the influence of cell shape anisotropy on the mechanical performance of closed cell aluminium foams using micro-computed tomography

A.-H. BENOUALI
Ecole des mines de Paris/CNRS, Centre des matériaux/UMR 7633, BP 87, 91003 Evry, France; K.U. Leuven, Department of Metallurgy and Materials Engineering (MTM), Kasteelpark Arenberg 44, B-3001 Heverlee, Belgium
E-mail: benouli@mat.ensmp.fr

L. FROYEN
K.U. Leuven, Department of Metallurgy and Materials Engineering (MTM), Kasteelpark Arenberg 44, B-3001 Heverlee, Belgium

T. DILLARD, S. FOREST, F. N'GUYEN
Ecole des mines de Paris/CNRS, Centre des matériaux/UMR 7633, BP 87, 91003 Evry, France
E-mail: samuel.forest@ensmp.fr

The mechanical behaviour of closed-cell aluminium foams made by both powder metallurgy (LKR) and liquid state (Hydro) processes is investigated. Hydro foams exhibit a significant anisotropy in their mechanical behaviour. The transverse direction stands out as the most favourable one in terms of strength. In contrast, LKR foams show an almost isotropic compressive behaviour. Both foams perform at a level far below the theoretical predictions. The reduced values are a result of imperfections and defects in the cellular microstructure. X-ray microfocus computed tomography (μCT) is therefore used for internal investigation of the foam cell structure. 2D and 3D quantitative image analyses have been performed on μCT images to characterise the morphometric parameters of the foams. The main parameters of interest are cell size, cell size distribution and cell features information. A preferred cell orientation in Hydro foams is observed along the normal and the transverse directions of the specimen. This cell shape anisotropy is quantified using the dimensions of the three axes of the equivalent ellipsoids. The orientation of the cells is well characterised by pole figures of the three axes of equivalent ellipsoids. The influence of this geometrical anisotropy on the mechanical behaviour of the foam is discussed.

1. Introduction

The past few years have seen an increasing interest in metal foams, especially made of aluminium or aluminium alloys. The stimulus for this lies in recent process developments, which promise materials with better quality and lower cost. On the other hand, foams are known to have many interesting combinations of physical and mechanical properties [1–3]. The efficient use of aluminium foams requires however, a detailed understanding of their mechanical behaviour as well as an appropriate microstructural characterisation.

Metal foams are often anisotropic, i.e. their properties depend on the direction in which they are measured. The heterogeneity and anisotropy measured in foams is generally attributable to the processing methods used in their production [1, 4, 5]. The anisotropy and orientation of the foam cells also affect the mechanical properties, so they cannot be ignored in engineering design. For this purpose the compressive behaviour of closed-cell aluminium foams is investigated regarding the specimen orientation.

The cell shape anisotropy is conveniently measured by the ratio of the largest cell dimensions to the smallest. The aim of this work is to provide quantitative information on the cell foam morphology, regarding the shape, size and orientation of the most representative cells and the corresponding statistics. Resolving the structure of cellular foams has been subject of scientific

0022-2461
DOI: 10.1007/s10853-005-4994-9

research for many years. However, recent observations using X-ray micro-computed tomography (μCT) have shown that this technique is particularly suitable for internal investigation and quality control of metal foams [6–8]. μCT is therefore used to provide input images for quantitative 3D image analysis.

2. Materials and methods

2.1. Specimens

Closed cell aluminium foams investigated in this study were produced by two different techniques. A powder metallurgical process (LK Ranshofen, Austria) and a liquid state route by melt gas injection (Norsk-Hydro, Norway).

The powder metallurgical process is based on the Alulight®-technique [3, 9]. Aluminium alloy is prepared by mixing metal powder and a foaming agent (typically titanium hydride). The content of the foaming agent depends on the metal to be foamed and the desired density. This precursor material is chopped into small pieces, placed inside a sealed split mould, and heated to temperatures above the melting point of the metal matrix. The metal melts and the foaming agent releases gas in a controlled way, creating voids with a high internal pressure. These expand by semi-solid flow and the aluminium swells, allowing the created foam to fill the mould. The process results in components with the same shape as the container. After the mould is filled, the process is stopped by simply allowing it to cool to a temperature below the melting point of the metal. The foam has closed cells with diameters that range from 1 to 5 mm and densities between 0.2 and 0.55 g/cm^3. The density of the metal foams is controlled by adjusting the content of the foaming agent and by varying the heating conditions.

In the continuous foam-casting route [3, 10], gas is dispersed into small bubbles in an aluminium composite melt by rotor impellers. The walls of the created bubbles are stabilised by dispersed refractory particles avoiding coalescence between them. The bubbles rise to the surface where they accumulate. The accumulated foam on the melt surface is then transferred to a conveyor belt, where it solidifies and cools. The melt may constitute of different alloys and refractory particles. The densities of aluminium foams produced this way range from 0.1 to 0.5 g/cm^3 with average pore sizes from 25 down to 3 mm. The density is controlled by the process parameters, the most important being the rotor speed, the gas flow through the rotor and the amount of particles in the melt.

Hydro foams were supplied in large panels from which specimens were cut. The foam was made from an AlSi7Mg alloy with approximately 10% volume fraction of 20 μm SiC particles. LKR foams were made from the cast aluminium alloy AlMg1Si0.6 (wt%). They were available in smaller cubic blocks of 100 mm side, from which test specimens were cut. The Hydro and LKR materials all had a solid skin on the outer surfaces, which was removed before testing. Specimens were cut using band sawing followed by milling of the surface. The density of individual specimens was calculated by weighing the specimens on an electronic balance and measuring their dimensions using a digital calliper. A wide range of densities was tested in compression for both Hydro and LKR foams.

2.2. Mechanical testing

Compression tests were carried out on cubic specimens. The size of the specimens for both foams was typically 50 × 50 × 50 mm^3. To avoid edge effects, the sample dimensions exceed at least seven cell diameters [2, 11, 13]. The Hydro material was loaded in three perpendicular directions (see Fig. 1a). We define the material axes of Hydro foams such that the longitudinal direction RD is the direction of the conveyor motion, the normal direction ND is parallel to the thickness of the panel, and the transverse direction TD is in the plane of the sheet, perpendicular to the conveyor motion. In contrast, since there was no preferred axis of cell elongation in LKR foams (see Section 3.1) and there was no indication of the orientation of the specimens from the manufacturer, few specimens of typically 50 × 50 × 50 mm^3 were cut from cubic blocks of 100 mm side. These specimens then were compressed in three different orthogonal directions regarding their previous orientation in the cuboid block as it is sketched in Fig. 1b.

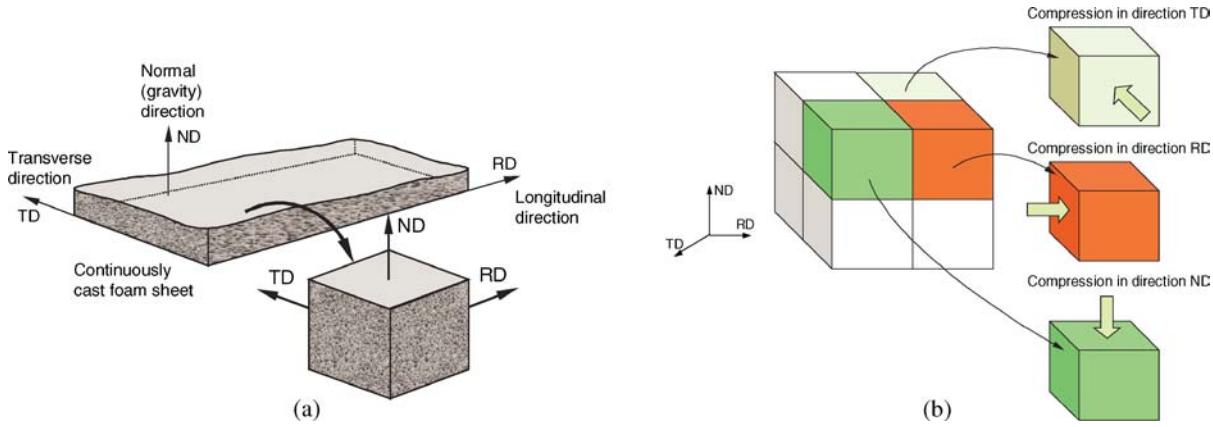

Figure 1 Reference systems for (a) Continuously cast sheet Hydro foam and (b) Compression of LKR foam samples in three orthogonal directions regarding to their initial position in the foam block.

Uniaxial compression tests were performed by deforming the specimen between two parallel steel platens to large nominal strains (up to 80%), in a servo-hydraulic machine equipped with a 100 kN load cell. The displacement was measured by two linear voltage displacement transducers (LVDT) on either side of the specimen up to a strain of approximately 5%; at higher strains the displacement was measured from the machine crosshead displacement. The displacement rate was 0.5 mm/min up to a strain of approximately 5%, while at higher strains, the rate was increased to 50 mm/min. The Young's modulus of the foam was calculated from the slope of the unloading load-deflection curve taken at approximately 75% of the expected plastic collapse stress of the foam, which was found from preliminary tests [4, 12]. The plastic collapse stress was calculated from the initial peak load on the specimen. In the case where no such yield points can be observed and the stress-strain curve increases sufficiently smoothly, one can extrapolate the plateau regime to zero deformation ($\varepsilon = 0$) and define compression strength this way [4, 14].

2.3. X-ray micro-computed tomography

Aluminium foam cell structure was investigated using the X-ray micro-computed tomography (μCT) facilities available at the department of metallurgy and materials Engineering (K.U. Leuven). It consists in the AEA Tomohawk tomography system associated with the Philips HOMX 161 X-ray microfocus source.

The principle of μCT is based on X-ray attenuation inside an object. The attenuation depends on the atomic number, density and thickness of the sample and on the energy of X-ray beam. A schematic sketch showing the basis of μCT technique is given in Fig. 2. The object to be inspected is mounted on a turntable. Rotation and translations are controlled par stepping motors. A conical X-ray beam is generated from an X-ray source and focused on a detector located on the opposite side of the specimen. After traversing the sample, the beam is recorded by a detector consisting in a fluorescent screen coupled with a 1024 $\times$ 1024 CCD (charge coupled device) camera. A total of 374 projections are needed to fully construct the two-dimensional cross-sections. These are obtained by rotating the object through 180 degrees. The final image is reconstructed using back projection algorithms [15]. The μCT images obtained by this method represent cross-sectional slices through the specimen in a horizontal plane perpendicular to the rotation axis of the turntable.

A full 3D volumetric μCT has been performed on Hydro and LKR cubes of typical side size of 50 mm. The density of Hydro and LKR foams were measured to be 0.19 g/cm^3 and 0.24 g/cm^3 respectively. The scanned 3D volumes were 50 $\times$ 50 $\times$ 26 mm^3. The X-ray beam energy was set to 21 keV. A complete scan lasts approximately 20 minutes and a minimum resolution of 90 μm was achieved. This resolution was sufficient to distinguish the cell walls in the density range of the investigated Hydro and LKR foams. Simone *et al.* [4] have measured an average cell wall thickness around 100 μm for Alcan foams with density ranging from 0.16 to 0.38 g/cm^3. LKR foams have however a thicker cell walls. 2D and 3D quantitative information on the cell morphology were carried out using image analysis.

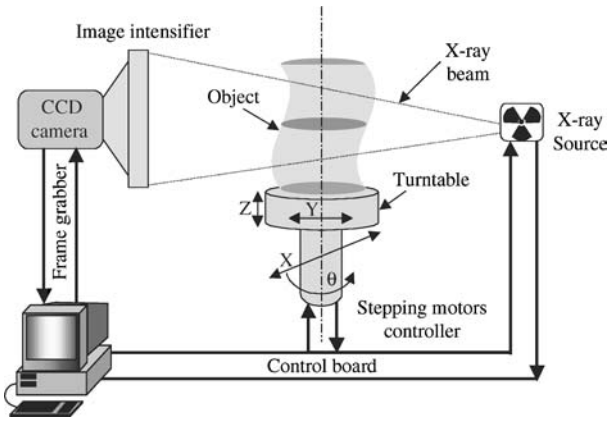

Figure 2 Working principle of the X-ray microfocus computed tomography.

3. Results and discussion

3.1. Qualitative description of the foam cell structure

Images of μCT slices of both Hydro and LKR foams in three orthogonal planes of the reference system described in Section 2.2 are given in Fig. 3 and 4.

Hydro Al-foams show heterogeneities and imperfections in their structure. The pictures reveal a broad cell size distribution leading to a broad local density distribution throughout the sample. Regions with high density consist of few large cells surrounded by many small ones. On the other hand, many faces have non-uniform curvature or are corrugated, and have occasional broken walls that still hang in place leading to form large elongated cells with their neighbours. The curved cell walls found in Hydro foams between adjacent cells of different sizes, are the result of both the cell size distributions in the foams when they were solidified and the buoyancy caused by air convection. As stated by Simone *et al.* in their comprehensive study on Alcan foam structure [4], the face corrugations observed in the cell walls of Hydro foams (see Fig. 3) are possibly caused either by shrinkage of the cell wall solid during solidification, or by the partial collapse of the newly solidified, but still soft, cell walls during production or under the weight of the foam itself. These wrinkled walls are more in evidence in the lower density foams with large cells.

The LKR foams in contrast were found to have an apparently isotropic and homogeneous cellular structure in terms of cell size as it is shown in Fig. 4. However, many of the cell walls in LKR foams are fractured, leading to a high connectivity parameter of the foams [7]. McCullough *et al.* [16] found from scanning electron microscopy (SEM) examination on Alulight foams produced the same way as LKR foams that cracks and voids are present in about one third of the cell faces.

One can also see that the cells are oriented in a preferred direction in Hydro foams while they are

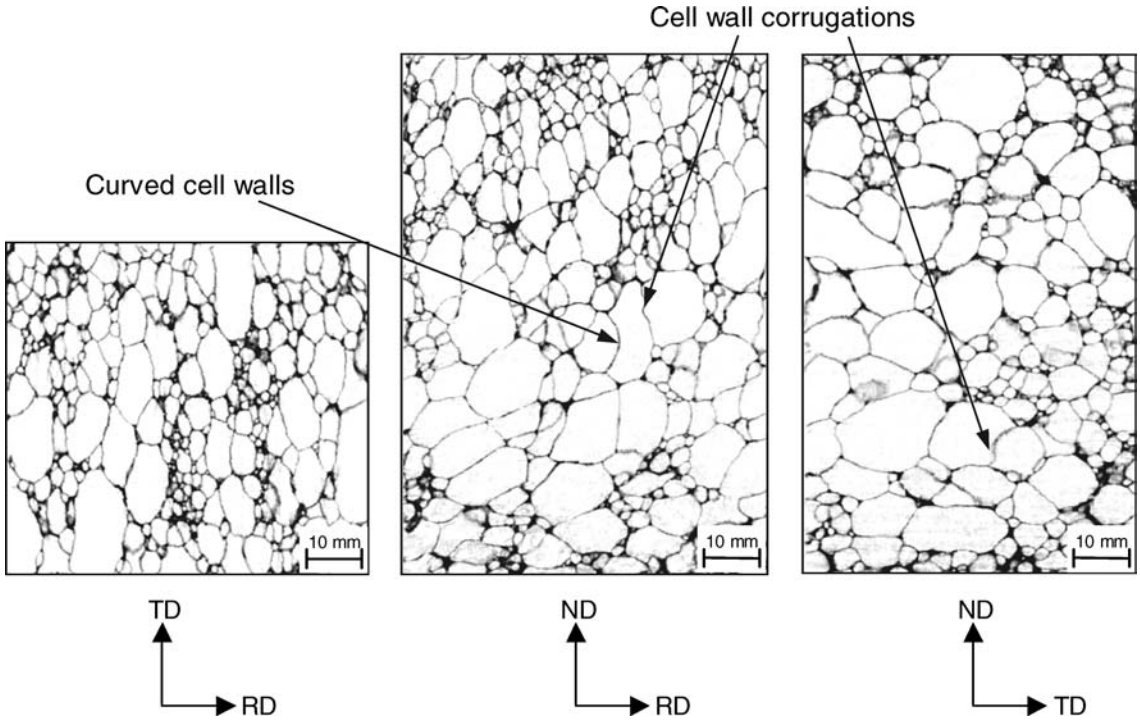

Figure 3 μCT slices of Hydro foam material of average density 0.19 g/cm^3 in three orthogonal planes of the reference system.

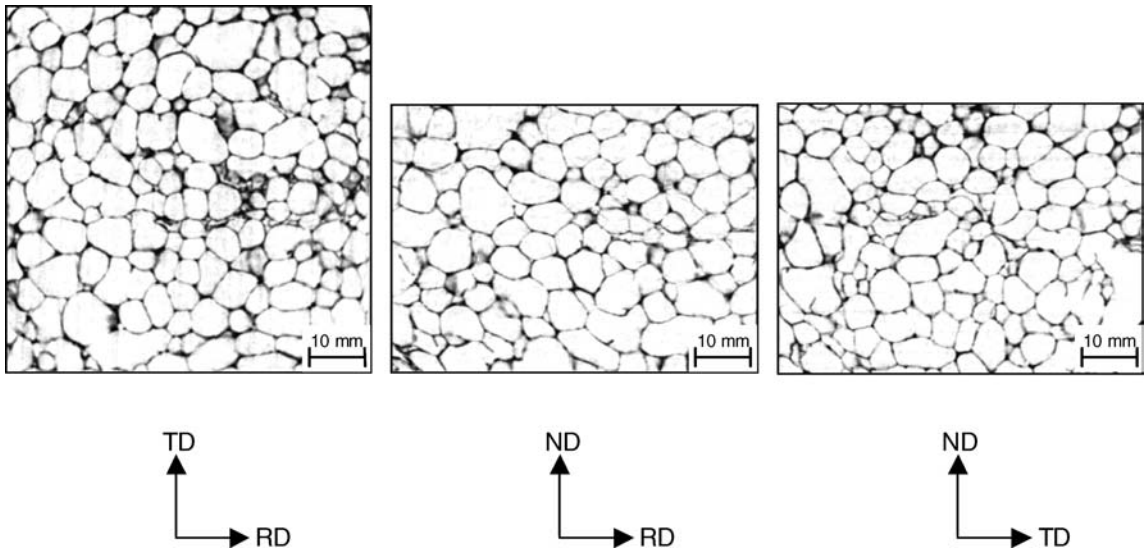

Figure 4 μCT slices of LKR foam material of average density 0.24 g/cm^3 in three orthogonal planes of the reference system.

randomly oriented in LKR foams. The observed heterogeneity and anisotropy in the Hydro foam panels (see Fig. 3) was described in details by Simone *et al.* [4]. This anisotropy in cell shape and orientation is directly related to the processing route used in their production. Indeed, in addition to the variation in cell wall thickness (and thus relative density) caused by drainage, the anisotropy of the cellular structure and the variation of anisotropy through the panels are due to the viscoplastic deformation of the liquid foam prior to solidification [4, 17, 18]. When the stabilized liquid foam in the Hydro process is conveyed mechanically from the melt, the greater weight carried by the cells at the bottom of the liquid foam slab causes increased pressure and thus, a smaller cell size with a flattened shape. Cells are also sheared in the longitudinal direction RD by the conveyor motion and stretched vertically in ND direction by convection of the air contained in the cells. The shearing effect influences the whole thickness of the slab. Nevertheless, the influence of overhead pressure is dominating at the bottom of the slab. This is also the case of air convection which dominates at the top of the slab [4].

3.2. Mechanical behaviour

Typical compressive stress-strain curves for Hydro and LKR foams are shown in Figs. 5 and 6. All curves display a first regime wherein the deformation is nominally linear. A stress maximum is then observed, corresponding to the onset of global collapse, followed by a region of strain softening to a plateau, at which successive bands of cells collapse and densify, with subsequent stress oscillations about a gradual overall

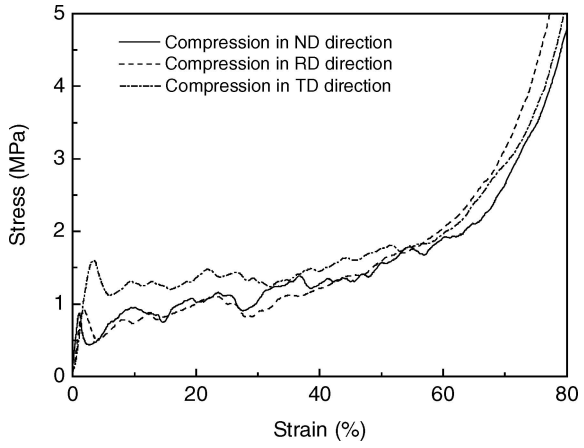

Figure 5 Anisotropic compressive behaviour of Hydro foam samples of average density of 0.19 g/cm^3 loaded in the three orthogonal directions of the reference system.

strain hardening until the entire densification of the foam material.

The plateau regions exhibit however, some differences among the studied foams. LKR foams deform smoothly throughout the entire strain range which is characteristic of a ductile behaviour. Their plateau stress also gradually increases with the strain. In contrast, the stress plateau of Hydro foams is serrated, as is typical in brittle foams. These serrations correspond to the fracture of cell walls as observed during testing.

Compression curves of Fig. 5 also show a significant variation in the compressive strength properties with specimen orientation for Hydro foams. The foam exhibits thereby a strong anisotropy in its mechanical behaviour. In this respect, it is evident that the TD direction stands out as the most favourable one in terms of strength, followed by the ND and RD directions. Indeed, the strength and the stiffness in the longitudinal and through-thickness directions are comparable and are approximately 50% lower than that in the transverse direction. One reason for this can be sought from the cell shape and cell orientation anisotropy discussed in Sections 3.1. This anisotropy is found to have the same order as the sequence of initial strengths found here (TD > ND > RD). That is, the cells have the major extension along the TD axis followed by the ND and RD axes, respectively. The theoretical approach by Gibson and Ashby [1] supports this observation, predicting the highest strength for the direction exhibiting the largest cell shape anisotropy ratio. The same observations were made by various researchers in the literature [4, 13, 16, 19–21]. Moreover, the stress-strain compressive curves of LKR specimens in the three orthogonal directions specified in Section 2.2 did not show a discernable effect of sample orientation (see Fig. 6). We emphasize that LKR foams exhibit an isotropic compressive behaviour.

Fig. 7a and b summarise the measured elastic modulus E^* and yield strength σ^*_{pl}, normalized by those of the solid alloy, and plotted against relative density. A power-law dependence of both E^* and σ^*_{pl} upon the relative density is noted, with an exponent in the range 1.65 – 2.5 for elastic modulus, and in the range

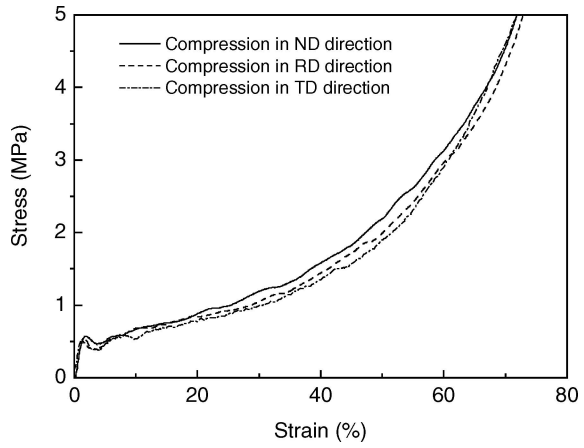

Figure 6 Isotropic compressive behaviour of LKR foam samples of average density of 0.24 g/cm^3 loaded in three different orthogonal directions.

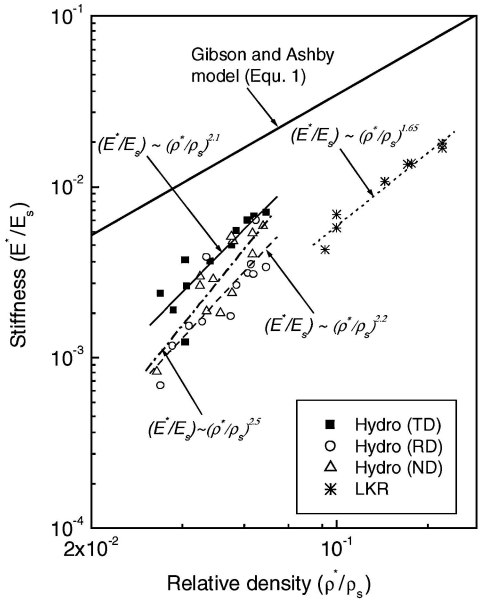

(a)

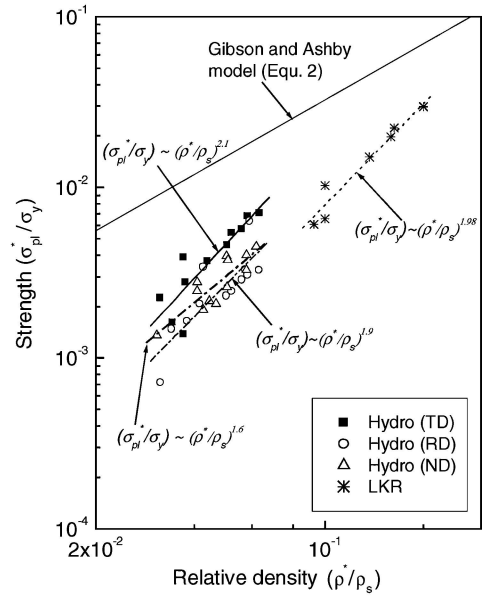

(b)

Figure 7 Effect of relative density upon (a) elastic modulus, and (b) compressive plateau strength for Hydro and LKR foams.

1.6 – 2.1 for strength. The experimental results show a significant scatter, particularly for Hydro foams. The scatter appears to be associated with the high degree of heterogeneity of the microstructure in Hydro foams, as well as the strong gradient of density in the thickness direction, as reported in Section 3.1. These observations are consistent with those reported by Simone *et al*. [4] and Olurin *et al*. [19].

The mechanical properties of closed cell foams are related to the mechanics of cell edge bending, and cell face stretching. Using an idealized cubic cell model Gibson and Ashby [1, 2] derived equations for design with cellular solids in terms of the foam relative density and properties of the material of which the foam is made. The contribution from cell face stretching to the overall stiffness and strength of the foam is by a term that is linear in the relative density, while the contribution from cell edge bending is non-linear in the relative density. Thus, the elastic modulus E^* of the foam is related to the elastic modulus of the cell wall material E_s according to

$$\frac{E^*}{E_s} = \phi^2 \left(\frac{\rho^*}{\rho_s}\right)^2 + (1-\phi)\frac{\rho^*}{\rho_s} \qquad (1)$$

where ϕ is the fraction of solid that is contained in the cell edges ($\rho^*/\rho_s \leq \phi \leq 1$), the remaining fraction $(1-\phi)$ occupies the cell faces.

Similarly, the yield strength of a foam σ^*_{pl} is expressed in terms of the yield strength of the cell wall material σ_{ys} by

$$\frac{\sigma^*_{pl}}{\sigma_{ys}} = 0.3\phi^{3/2}\left(\frac{\rho^*}{\rho_s}\right)^{3/2} + (1-\phi)\frac{\rho^*}{\rho_s} \qquad (2)$$

The prediction models for the stiffness and strength given by equations 1 and 2 require the mechanical properties of the cell wall material. The density and elastic modulus of the solid aluminium alloys were taken to be the reference value for aluminium [1] (2.7 g/cm^3 and 70 GPa respectively). The cell wall yield strength was taken to be 250 MPa for Hydro foams and 130 MPa for LKR material, both are reference values given by the manufacturers [9, 10]. The distribution constant ϕ varies with the foam density. Usually, values between 0.65 and 0.85 are commonly observed [7, 16]. ϕ was however set to 0.75 for comparison purposes. Table I shows a comparison between the predicted and measured stiffness and strength. It is clear that the stiffness and strength of the two foams are significantly less than the predictions (1) and (2). These equations, in fact were derived and validated for polymeric foams. The discrepancy is related to the high level of imperfection within the foam cell structure as described in Section 3.1. These defects consist in cell wall curvature and corrugations, porous inclusions, holes and fractured cell walls as well non-uniform distribution of local density [4, 16, 22, 23].

3.3. Quantitative 2D and 3D characterization of the foam cell structure

For a complete characterization of the cell shape and to provide quantitative morphological data, a 3D segmentation of the cells is necessary. The 3D starting volume, derived from one μCT, is divided into a set of 2D grey tone slices. An appropriate threshold is then applied to generate binary images on which a segmentation process is applied using a watershed procedure.

3.3.1. 3D segmentation procedure

A 3D image analysis algorithm originally developed for the measurement of pore size distribution in soils [8, 24, 25], has been adapted for 2D and 3D quantitative measurement of the foam cell features. The 3D segmentation routine is divided into three main steps.

TABLE I Comparison of the predicted and measured values for stiffness and strength (mean (standard deviation))

			Predicted		Measured	
Material direction	Density (g/cm^3)	Relative density	E (MPa)	σ_{pl} (MPa)	E (MPa)	σ_{pl} (MPa)
Hydro						
TD	0.08	0.03	560	2.13	149 (23)	0.49 (0.11)
RD					65 (24)	0.28 (0.13)
ND					58 (20)	0.34 (0.15)
TD	0.10	0.04	763	2.89	177 (87)	0.68 (0.32)
RD					114 (7)	0.50 (0.08)
ND					148 (32)	0.54 (0.07)
TD	0.13	0.05	937	3.67	320 (65)	1.15 (0.21)
RD					225 (43)	0.73 (0.12)
ND					214 (48)	0.68 (0.12)
TD	0.16	0.06	1192	4.47	469 (25)	1.64 (0.18)
RD					286 (107)	1.00 (0.39)
ND					370 (32)	1.01 (0.04)
LKR						
	0.26	0.10	2144	7.79	454 (139)	1.21 (0.50)
	0.37	0.15	3511	12.20	754 (25)	1.96 (0.93)
	0.44	0.16	3808	13.12	954 (13)	2.73 (0.23)
	0.54	0.20	5075	16.86	1217 (52)	3.86 (0.03)

First, the image skeleton is calculated by means of local aperture distributions corresponding to the diameter of the subscribed circles inside the cell borders. A distance map image of the cells is then computed, it represents the distance to the cell edges for each point of the cell volume. Finally by selecting the local maximums from the distance map a watershed procedure is applied to separate the cells. In the resulting image or volume all individual cells are separated and labelled allowing to directly characterizing the desired morphometric parameters of the cells that are not connected with the borders of the investigated volume. Fig. 8a and 8b represent a 3D rendering of μCT slices of Hydro and LKR foams and the corresponding results obtained from the 3D segmentation procedure.

3.3.2. Quantitative 2D image analysis: Geometrical versus mechanical anisotropy in longitudinal and transverse planes in Hydro foams

As stated in Section 3.1, the heterogeneity and anisotropy measured in the Hydro foam panels is attributable to the processing methods used in their production. Hydro foams exhibit a visually discernible gradient in cell size, shape and orientation through the thickness of the foam. They also have a discernibly different cellular structure in the longitudinal and transverse sections. Following the same methodology used by Simone *et al*. [4], quantitative 2D image analysis procedure was used for the investigation of the variations of cell structure through the thickness of the sample in (TD, ND) and (RD, ND) planes. This is conducted by plotting properties of the best-fit ellipses as a function of position in the specimen cross-section. The boundaries between sub-strata represented by white dashed lines on Fig. 9 were defined by a sharp change in the gradient of the orientation of the cells. The best-fit ellipse for each cell was defined as the ellipse having the same area and moments of inertia about the calculated principal axes. The major and minor axis lengths, a and b, and the major axis orientation, θ, were recorded. 27 cross-sections were analysed in each plane leading in a total number of more than 3000 cells. The ellipse fit to each sub-strata of the Hydro foam in the longitudinal and transverse planes are shown in Fig. 9. In the longitudinal plane, the cell orientation rotates from nearly horizontal at the bottom of the sheet to nearly vertical at the top with only slight changes in cell size and shape. In contrast, in the transverse plane, the orientation remains roughly horizontal, but the cells increase in size and become more rounded from the bottom to the top of the panel.

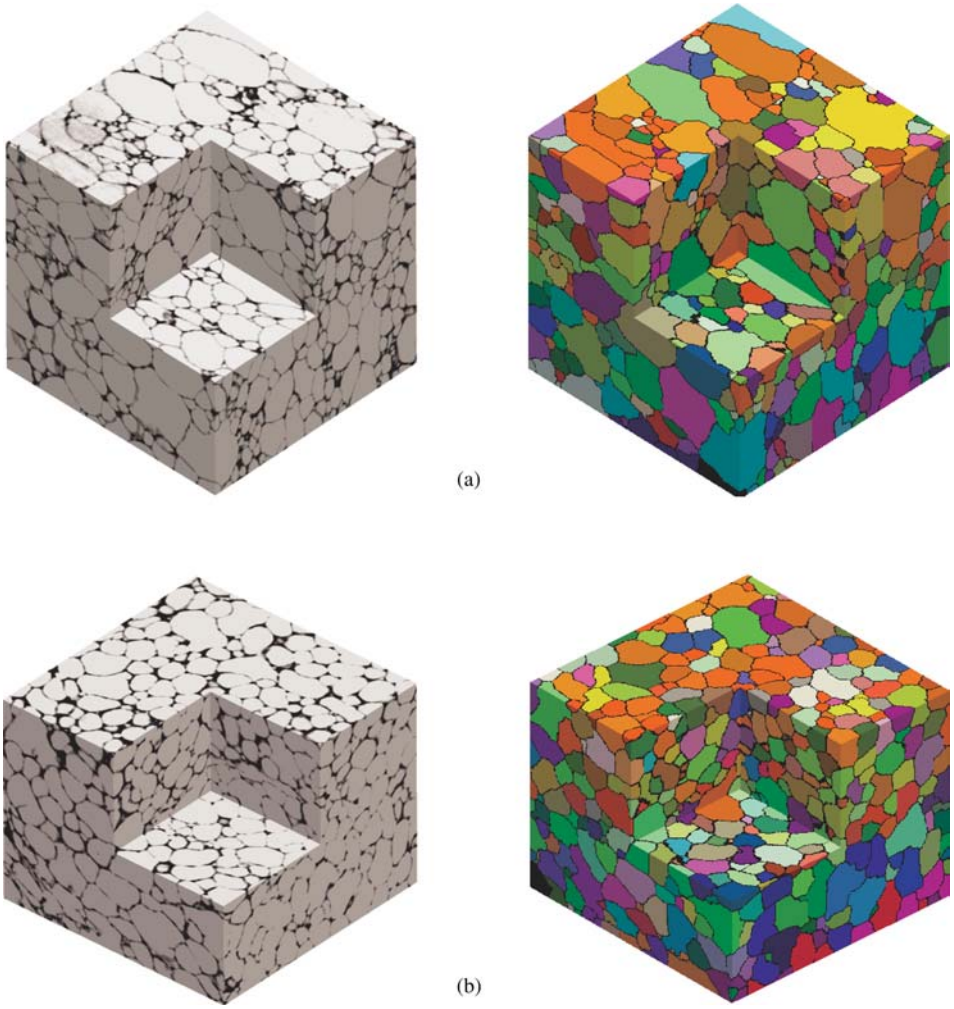

Figure 8 3D rendering of the μCT slices and the corresponding result of 3D segmentation procedure for (a) Hydro foam of average density 0.19 g/cm^3 and (b) LKR specimen of average density 0.24 g/cm^3.

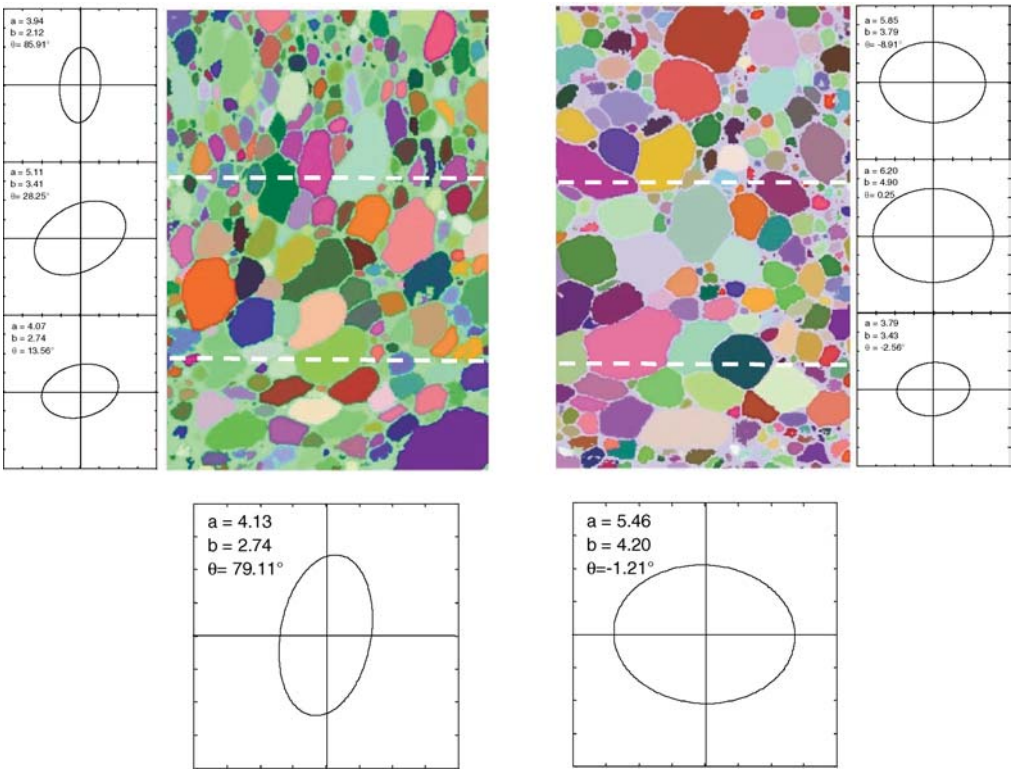

Figure 9 Results of 2D image analysis on Hydro foams showing the regional fabric ellipse summary for (a) longitudinal and (b) transverse planes.

One can see that the average best-fit ellipse is oriented horizontally parallel to the transverse direction in (TD, ND) plane whereas it is more likely oriented vertically perpendicular to the longitudinal direction in the plane (RD, ND). A possible explanation for the highest strength when loading in TD direction is related to the cell shape and orientation in (TD, ND) plane. Indeed, the average best-fit ellipse in (TD, ND) cross-sections presents an "equiaxed" morphology with minimal ellipticity, the orientation of its major axis parallel to the loading direction, TD, suggests that the cells would deform by buckling. In contrast, the best-fit ellipse in (RD, ND) plane is more elongated, its major axis is oriented perpendicular to the loading direction, RD, which allow the cell wall junctions to bend easily initiating by the way band formation observed in compression and thus leading to a lower strength than that observed in TD direction. This is consistent with the observations made by Bart-Smith *et al*. [6] on the yielding mechanisms in ALPORAS foams using X-ray tomography. They stated that the shape anisotropy is more important than cell size in determining yielding susceptibility of the cells. We re-emphasise that cell orientation also appears to be of major importance.

3.3.3. Quantitative 3D measurements using equivalent ellipsoids

A quantitative 3D analysis of the cell morphology in Hydro and LKR foams is carried out. To obtain statistically representative results, large volumes are analysed. Incomplete cells at the boundaries are excluded during the analysis. The investigated volume for Hydro foams is 42 × 42 × 42 mm^3 containing about 500 cells while the studied LKR foam volume is 44 × 44 × 36 mm^3 containing about 700 cells.

3.3.4. Cell volume distribution

The volume of individual cells is determined by counting the voxels belonging to the cell. A marching cube algorithm is used to better estimate this parameter [26]. Fig. 10 shows the cell volume distributions for Hydro and LKR foams. The distributions are bimodal for both foams with a first peak centred on 25 mm^3 and a second one around large cells. However, it must be noticed that the proportion of small cells around the first peak in Hydro foams is about 60% higher than that in LKR foams. On the other hand, the proportion of large cells

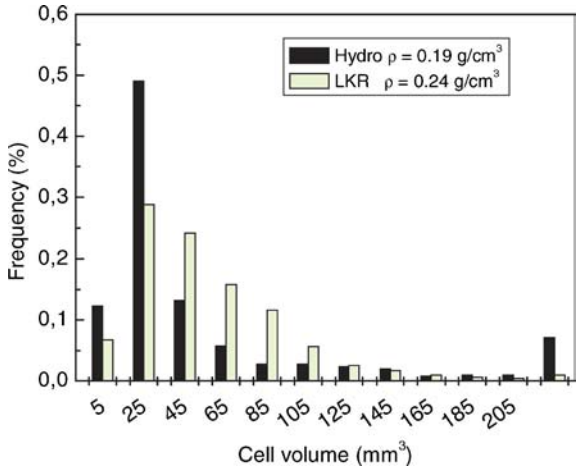

Figure 10 Histogram showing the cell volume distribution for Hydro and LKR foams (frequency in number).

in LKR foams is very low, it is about 5 times smaller than in Hydro material, which is characteristic of a more homogeneous cell size distribution through the specimen. This confirms the qualitative observation made in Section 3.1 (See Fig. 4).

3.3.5. Cell shape anisotropy

The cell shape anisotropy is investigated by replacing the cells by equivalent ellipsoids. 3D inertia matrix of the equivalent ellipsoid is determined for each cell. The eigen values of the matrix denoted $a < b < c$ associated with the eigen vectors are computed for each cell. Fig. 11a and b show the three mono–modal distributions of parameters a, b, and c for both Hydro and LKR foams. As expected, the three dimensions of the equivalent ellipsoid are different. The distribution of the small axes a of the equivalent ellipsoid is the least scattered while the distribution of the large axes c is the most scattered. Table II summarizes the main results obtained for Hydro and LKR foams. The average cell volume, the average length of equivalent ellipsoid axes, the aspect ratios and the sphericity factor F_{sph} are reported. The sphericity factor is a shape parameter given by: $F_{sph} = 6V(\pi / S^3)^{0.5}$, where S and V *are* the surface and the volume of the equivalent ellipsoid. This parameter is 1 for a sphere and less for every other shape. The aspect ratios for the average ellipsoid in Hydro foams are 1.91 between the largest and the smallest axes, 1.42 between the largest and medium axes and 1.35 between the medium and the smallest axes. That means that the cells are more elongated in one direction. In LKR foams the cell are more "equiaxed" the aspect ratios of the average ellipsoid are close to each other, 1.29 between the largest and smallest axes, 1.07 between the largest and medium axes and 1.20 between the medium and the smallest axes.

3.3.6. Cell orientation

In order to characterize the orientation of the cells, the same methodology described by Dillard *et al*. [27, 28] was applied. For this purpose, the eigen vectors of the moment of inertia matrix associated with the eigen values a, b, and c are computed and analysed. The stereographic projections of these vectors are represented in the plane (TD, RD) in Fig. 12 and 13 for Hydro and LKR foams respectively. The orientation of the ellipsoid axes of each cell for Hydro foams is represented by a black spot in the plane (TD, RD) of the pole Fig. 12. One can clearly see the preferred cell orientation in Hydro foams. Indeed the largest axes of the ellipsoid are aligned with TD direction while the smallest ones are rather in the direction RD. The medium axes stand with the ND direction. These results are in accordance with the ones made in Section 3.2 relative to the mechanical behaviour anisotropy. Indeed, It was found that the foam is stiffer in direction showing the largest shape anisotropy (TD direction). On the other hand no preferred orientation is observed for LKR foams in any of the planes. The stereographic projections of axes a, b and c exhibit a random spatial distribution in all the planes (see Fig. 13). This confirms the qualitative observation made on the corresponding μCT Slices in

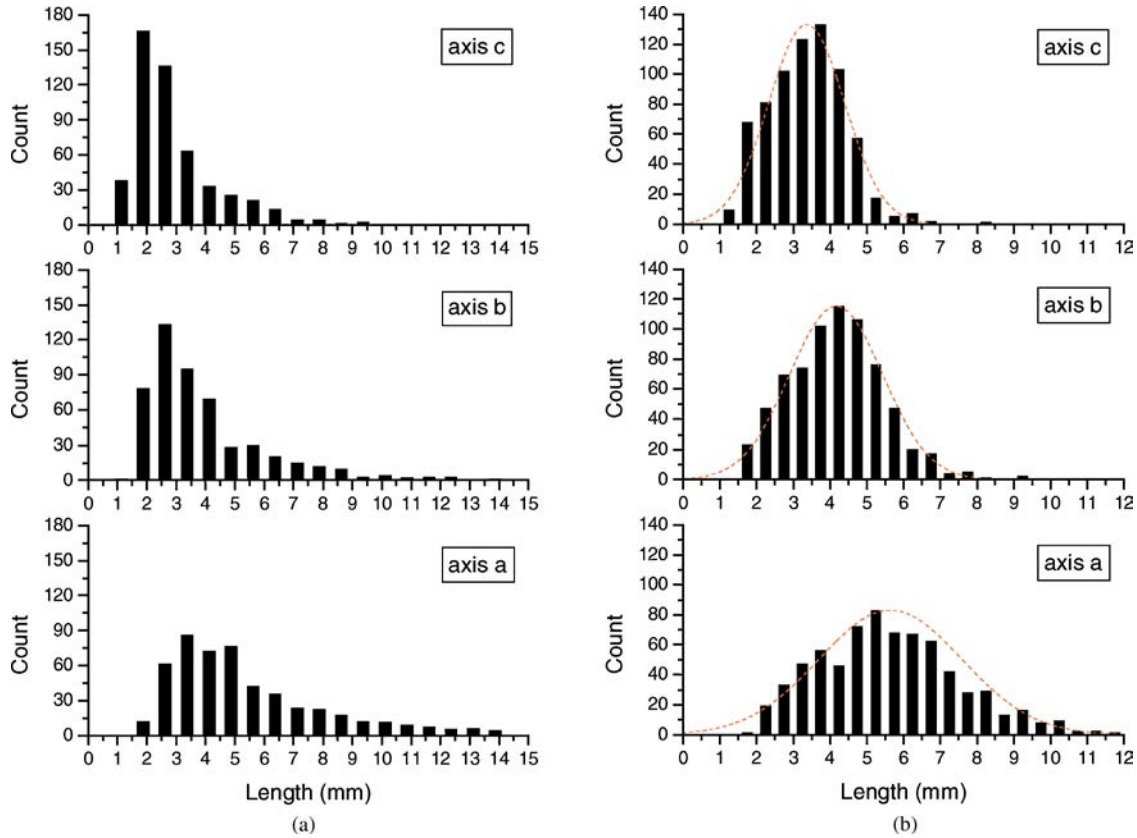

Figure 11 Histograms showing the length distributions of the axes of equivalent ellipsoids for cells at the initial stage for (a) Hydro foam of average density 0.19 g/cm^3 and (b) LKR specimen of average density 0.24 g/cm^3.

TABLE II Results of 3D quantitative measurement using equivalent ellipsoid (mean (standard deviation))

Foam	Density (g/cm^3)	Average cell volume (mm^3)	Average length a (mm)	b (mm)	c (mm)	Aspect ratios c/b	c/a	b/a	Sphericity
Hydro	0.19	57 (113)	2.90 (1.43)	3.93 (2.07)	5.51 (2.89)	1.42 (0.29)	1.91 (0.41)	1.35 (0.21)	0.68 (0.05)
LKR	0.24	47 (42)	3.97 (1.04)	4.25 (1.27)	5.11 (1.14)	1.20 (0.23)	1.29 (0.32)	1.07 (0.16)	0.87 (0.06)

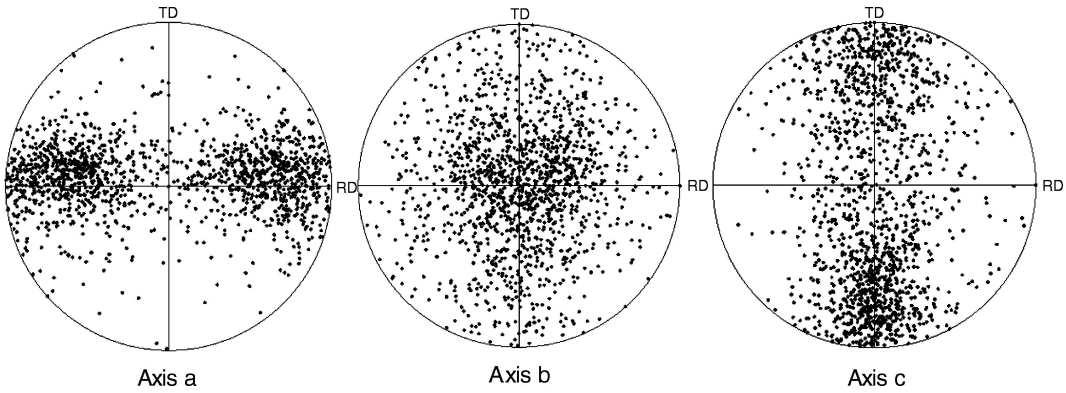

Figure 12 Orientation of the axes of the equivalent ellipsoids in the plane (TD, RD) for Hydro foams.

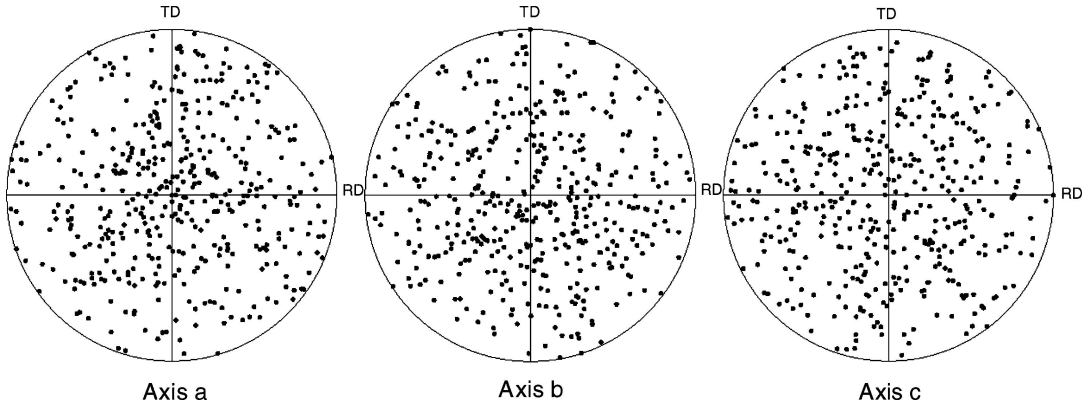

Figure 13 Orientation of the axes of the equivalent ellipsoids in the plane (TD, RD) for LKR foams.

Section 3.1 (see Fig. 4). It is also in accordance with the observed isotropic mechanical behaviour discussed in Section 3.2 (see Fig. 6).

4. Conclusions

In this study we have investigated the uniaxial compressive behaviour of closed-cell aluminium foams made by both powder metallurgy (LKR) and liquid state (Hydro) processes. Both foams have moduli and strengths that fall well below the theoretical predictions. The reduced values are a result of imperfections and defects in the cellular microstructure.

Qualitative observations using μCT images of Hydro and LKR foams show heterogeneities and imperfections in their structure. Hydro foams exhibit a visually discernible gradient in cell size, shape and orientation through the thickness of the foam and in the longitudinal and transverse planes. The LKR foams in contrast were found to have an apparently homogeneous cellular structure in terms of cell size. However the main observed defects are the cracks in the cell faces which explain their poor mechanical properties by their tendency to behave as open cell rather than closed cell foams.

LKR foams show an almost isotropic compressive behaviour whereas Hydro foams exhibit a significant anisotropy in its mechanical behaviour. The transverse direction, TD, stands out as the most favourable one in terms of strength.

The anisotropic compressive response in Hydro foams was related to the cell shape anisotropy and orientation. 2D quantitative image analysis revealed that in the transverse plane, the average cell has an "equiaxed" morphology with minimal ellipticity, and is oriented parallel to the loading direction TD. That suggests the cells would deform by buckling. In contrast, in the longitudinal plane the cells are elongated and oriented perpendicular to the loading direction RD which allow them to bend easily and thus leading to a lower strength than that observed in TD direction.

Quantitative 3D analysis of the cell morphology in Hydro and LKR foams was carried out using image analysis. The cell volume distributions are bimodal for both foams. The cell shape anisotropy was investigated by determining the dimensions and orientation of the equivalent ellipsoid for each cell. The corresponding aspect ratios for the average ellipsoid in Hydro foams are 1.91 between the largest and the smallest axes, 1.42 between the largest and medium axes and 1.35 between the medium and the smallest axes. In LKR foams the aspect ratios of the average ellipsoid are close to each other, 1.29 between the largest and smallest axes, 1.07 between the largest and medium axes and 1.20 between the medium and the smallest axes. A preferred cell orientation was found in Hydro foams. Indeed the longest axes of the ellipsoid are aligned with the transverse direction, TD while the smallest ones are rather in the longitudinal direction, RD. The medium axes stand with the normal direction, ND. This supports the mechanical behaviour anisotropy stating that the foam is stiffer in TD direction. In contrast, no preferred orientation was observed in LKR foams in any of the planes, that is in accordance with the observed isotropic mechanical behaviour of LKR foams.

Acknowledgements

The authors wish to acknowledge the financial support provided through the European Community's Human Potential Programme under contract HPRN-CT-2002-00198, [DEFINO].

References

1. L. J. GIBSON and M. F. ASHBY, in "Cellular solids" (Pergamon, Oxford, 1988).
2. M. F. ASHBY, A. G. EVANS, N. A. FLECK, L. G. GIBSON, J. W. HUTCHINSON and H. N. G. WADLEY, in "Metal foams: a design guide" (Butterworth–Heinemann, Boston, 2000).
3. J. BANHART, *J. Prog. Mater. Sci* **46** (2001) 559.
4. E. SIMONE and L. J. GIBSON, *Acta Mater.* **46** (1998) 3109.
5. A. T. HUBER and L. J. GIBSON, *J. Mater. Sci.* **23** (1988) 3031.
6. H. BART-SMITH, A. F. BASTAWROS, D. R. MUMM, A. G. EVANS, D. J. SYPECK and H. N. G. WADLEY, *Acta Mater.* **46** (1998) 3583.
7. A. ELMOUTAOUAKKIL, L. SALVO, E. MAIRE and G. PEIX, *Adv.Eng. Mater.* **4** (10) (2002) 803.
8. A. H. BENOUALI, L. FROYEN, J. F. DELERUE and M. WEVERS, *Mater. Sci. Tech.* **18** (2002) 489.
9. R. KRETZ, E. HOMBERGSMEIER and K. EIPPER, in Proceedings of International Conference on Metal foams and porous metal structures, Bremen, June 1999, edited by J. Banhart, M. F. Ashby, N. A. Fleck (MIT Press–Verlag, 1999) p. 23.
10. P. ASHOLT, in Proceedings of International Conference on Metal foams and porous metal structures, Bremen, June 1999, edited by J. Banhart, M. F. Ashby and N. A. Fleck (MIT Press–Verlag, 1999) p. 133.
11. E.W. ANDREWS, G. GIOUX, P. ONCK and L. J. GIBSON, *Int. J. Mech. Sci.* **43** (2001) 701.
12. E. ANDREWS, W. SANDERS and L. J. GIBSON, *Mater. Sci. Eng.* **A270** (1999) 113.
13. P. R. ONCK, E. W. ANDREWS and L. J. GIBSON, *Int. J. Mech. Sci.* **43** (2001) 681.
14. J. BANHART and J. BAUMEISTER, *J. Mater. Sci.* **33** (1998) 1431.
15. S. F. BURCH and P. F. LAWRENCE, *British Journal of NDT* **34** (3) (1992) 129.
16. K. J. G. MCCULLOUGH, N. A. FLECK and M. F. ASHBY, *Acta Mater.* **47** (1999) 2323.
17. D. WEAIRE and T. L. FU, *J. Rheol.* **32**(3) (1988) 271.
18. A. M. KRAYNIK and D. A. REINELT, *J. Coll. Inter. Sci.*, **181** (1996) 511.
19. O. B. OLURIN, N. A. FLECK and M. F. ASHBY, *Mater. Sci. Eng.* **A291** (2000) 136.
20. J. T. BEALS and M. S. THOMPSON, *J. Mater. Sci.* **32** (1997) 3595.
21. A. G. HANSSEN, O. S. HOPPERSTAD, M. LANGSETH and H. ILSTAD, *Int. J. Mech. Sci.* **44** (2002) 359.
22. M. J. SILVA and L. J. GIBSON, *ibid.* **39**(5) (1997) 549.
23. Y. SUGIMURA, J. MEYER, M. Y. HE, H. BART-SMITH, J. GRENSTEDT and A. G. EVANS, *Acta Mater.* **45** (12) (1997) 5245.
24. J. F. DELERUE, *Journal of Physics and Chemistry of the Earth* **24** (1999) 639.
25. S. BEUCHER, in Proceedings of International Conference on Applications of mathematical morphology in material sciences, Colmar, France, May 1995, p. 41.
26. W. E. LORENSEN and H. E. CLYNE, *Computer Graphics* **21**(4) (1987) 163.
27. T. DILLARD, F. N'GUYEN, E. MAIRE, S. FOREST, Y. BIENVENUE, J.-D. BARTOUT, M. CROSET, L. SALVO, R. DENDIEVEL and P. CLOETENS, *Philosophical Magazine* **85** (2005) 2147.
28. T. DILLARD, F. N'GUYEN, S. FOREST, Y. BIENVENUE, J.-D. BARTOUT, L. SALVO, R. DENDIEVEL, E. MAIRE, P. CLOETENS and C. LANTU'EJOUL, in Proceedings of International Conference on Metal foams and porous metal structures, Bremen, June 1999, edited by J. Banhart, M. F. Ashby and N. A. Fleck (MIT Press–Verlag, 1999) p. 301.

Received December 2004
and accepted April 2005